# On the origin of near-infrared extragalactic background light anisotropy

Michael Zemcov *et al.*

*Science* **346**, 732 (2014);
DOI: 10.1126/science.1258168

## REFERENCES AND NOTES

1. F. A. Lindemann, *Phys. Z.* **11**, 609 (1910).
2. M. Born, *J. Chem. Phys.* **7**, 591 (1939).
3. N. F. Mott, *Nature* **145**, 801–802 (1940).
4. J. L. Tallon, *Nature* **299**, 188 (1982).
5. D. Kuhlmann-Wilsdorf, *Phys. Rev.* **140**, A1599–A1610 (1965).
6. T. Gorecki, *Z. Metallkunde Mat. Res. Adv. Tech.* **65**, 426 (1974).
7. L. Gómez, A. Dobry, Ch. Geuting, H. T. Diep, L. Burakovsky, *Phys. Rev. Lett.* **90**, 095701 (2003).
8. X. M. Bai, M. Li, *Phys. Rev. B* **77**, 134109 (2008).
9. M. Volmer, A. Weber, *Z. Phys. Chem.* **119**, 277 (1926).
10. R. Becker, W. Döring, *Ann. Phys.* **416**, 719–752 (1935).
11. R. P. Sear, *Int. Mater. Rev.* **57**, 328–356 (2012).
12. T. Q. Yu, M. E. Tuckerman, *Phys. Rev. Lett.* **107**, 015701 (2011).
13. W. E, W. Ren, E. Vanden-Eijnden, *J. Phys. Chem. B* **109**, 6688–6693 (2005).
14. L. Maragliano, A. Fischer, E. Vanden-Eijnden, G. Ciccotti, *J. Chem. Phys.* **125**, 024106 (2006).
15. R. Lynden-Bell, J. Van Duijneveldt, D. Frenkel, *Mol. Phys.* **80**, 801–814 (1993).
16. M. Forsblom, G. Grimvall, *Nat. Mater.* **4**, 388–390 (2005).
17. Materials and methods are available as supplementary materials on *Science* Online
18. P. R. Couchman, C. L. Reynolds Jr., *Philos. Mag.* **34**, 327–329 (1976).
19. A. M. Alsayed, M. F. Islam, J. Zhang, P. J. Collings, A. G. Yodh, *Science* **309**, 1207–1210 (2005).
20. H. Rösner, B. Freitag, G. Wilde, *Philos. Mag. Lett.* **87**, 341–347 (2007).
21. Z. Wang, F. Wang, Y. Peng, Z. Zheng, Y. Han, *Science* **338**, 87–90 (2012).
22. E. Fukushima, A. Ookawa, *J. Phys. Soc. Jpn.* **10**, 970–981 (1955).
23. B. J. Siwick, J. R. Dwyer, R. E. Jordan, R. J. D. Miller, *Science* **302**, 1382–1385 (2003).
24. J. J. Gilvarry, *Phys. Rev.* **102**, 308–316 (1956).
25. Z. H. Jin, P. Gumbsch, K. Lu, E. Ma, *Phys. Rev. Lett.* **87**, 055703 (2001).
26. K. Sokolowski-Tinten *et al.*, *Nature* **422**, 287–289 (2003).
27. R. M. J. Cotterill, J. U. Madsen, *Nature* **288**, 467–469 (1980).
28. H. J. Fecht, W. L. Johnson, *Nature* **334**, 50–51 (1988).
29. R. W. Cahn, *Nature* **334**, 17–18 (1988).
30. J. W. Cahn, *Acta Metall.* **5**, 169–172 (1957).



## ACKNOWLEDGMENTS

Work by W.E and A.S. at Princeton was supported by the U.S. Department of Energy (DOE) (grant DE-SC0009248) and in Beijing by the National Natural Science Foundation of China (9130005). This work was partially performed under the auspices of DOE by Lawrence Livermore National Laboratory under contract DE-AC52-07NA27344. Work by M.E.T. was supported by NSF grant CHE-1301314.


## SUPPLEMENTARY MATERIALS

www.sciencemag.org/content/346/6210/729/suppl/DC1
Materials and Methods
Figs. S1 to S7
References (*31*–*41*)

24 March 2014; accepted 10 October 2014
10.1126/science.1253810

EARLY UNIVERSE

# On the origin of near-infrared extragalactic background light anisotropy

**Michael Zemcov,[1,2] Joseph Smidt,[3,4] Toshiaki Arai,[5,6] James Bock,[1,2]* Asantha Cooray,[4] Yan Gong,[4] Min Gyu Kim,[7] Phillip Korngut,[2,1] Anson Lam,[8,1] Dae Hee Lee,[9] Toshio Matsumoto,[5,10] Shuji Matsuura,[5] Uk Won Nam,[9] Gael Roudier,[2] Kohji Tsumura,[11] Takehiko Wada[5]**

**Extragalactic background light (EBL) anisotropy traces variations in the total production of photons over cosmic history and may contain faint, extended components missed in galaxy point-source surveys. Infrared EBL fluctuations have been attributed to primordial galaxies and black holes at the epoch of reionization (EOR) or, alternately, intrahalo light (IHL) from stars tidally stripped from their parent galaxies at low redshift. We report new EBL anisotropy measurements from a specialized sounding rocket experiment at 1.1 and 1.6 micrometers. The observed fluctuations exceed the amplitude from known galaxy populations, are inconsistent with EOR galaxies and black holes, and are largely explained by IHL emission. The measured fluctuations are associated with an EBL intensity that is comparable to the background from known galaxies measured through number counts and therefore a substantial contribution to the energy contained in photons in the cosmos.**

At near-infrared wavelengths, where the large zodiacal light foreground complicates absolute photometry measurements, the extragalactic background light (EBL) may be best accessed by anisotropy measurements. On large angular scales, fluctuations are produced by the clustering of galaxies, which is driven by the underlying distribution of dark matter. EBL anisotropy measurements can probe emission from epoch of reionization (EOR) galaxies (*1*–*3*) and direct-collapse black holes (*4*) that formed during the EOR before the universe was fully ionized by exploiting the distinctive Lyman cutoff feature in the rest-frame ultraviolet (UV), thus probing the UV luminosity density at high redshifts (*5*). However, large-scale fluctuations may also arise from the intrahalo light (IHL) created by stars stripped from their parent galaxies during tidal interactions (*6*) at redshift $z < 3$. A multiwavelength fluctuation analysis can distinguish among these scenarios and constrain the EOR star formation rate.

A search for such background components must carefully account for fluctuations produced by known galaxy populations. Linear galaxy clustering is an important contribution to fluctuations on scales much larger than galaxies themselves. On fine scales, the variation in the number of galaxies produces predominantly Poissonian fluctuations, with an amplitude that depends on the luminosity distribution. Anisotropy measurements suppress foreground galaxy fluctuations by masking known galaxies from an external catalog.

The first detections of infrared fluctuations in excess of the contribution from known galaxies with the Spitzer Space Telescope (*7*–*9*) were interpreted as arising from a population of faint first-light galaxies at $z > 7$. The Hubble Space Telescope was used at shorter wavelengths (*10*) to carry out a fluctuation study in a small deep field but did not report fluctuations in excess of known galaxy populations. Measurements with the AKARI satellite (*11*) show excess fluctuations with a blue spectrum rapidly rising from 4.1 μm to 2.4 μm. Fluctuation measurements in a large survey field (*6*) with Spitzer agreed with earlier measurements (*7*–*9*) but were instead interpreted as arising from tidally stripped stars at $z \sim 1$ to 3. Most recently, a partial correlation has been reported (*12*) between Spitzer and soft x-ray images, which Yue *et al.* (*4*) interpret as arising from direct-collapse black holes at $z > 12$.

We have developed and flown the specialized Cosmic Infrared Background Experiment [CIBER (*13*)], a rocket-borne instrument specifically designed to study the spatial and spectral properties of the EBL. The imaging instrument (*14*) measures fluctuations in $\Delta\lambda/\lambda = 0.5$ bands centered at 1.1 and 1.6 μm using two 11-cm telescopes each with a 2° by 2° field of view. Here, we report our analysis of data from two flights in 2010 and 2012.

The CIBER imager data are reduced from raw telemetered time streams, flat-field–corrected based

[1]Department of Physics, Mathematics, and Astronomy, California Institute of Technology, Pasadena, CA 91125, USA. [2]Jet Propulsion Laboratory (JPL), National Aeronautics and Space Administration (NASA), Pasadena, CA 91109, USA. [3]Theoretical Division, Los Alamos National Laboratory, Los Alamos, NM 87545, USA. [4]Department of Physics and Astronomy, University of California, Irvine, CA 92697, USA. [5]Department of Space Astronomy and Astrophysics, Institute of Space and Astronautical Science (ISAS), Japan Aerospace Exploration Agency (JAXA), Sagamihara, Kanagawa 252-5210, Japan. [6]Department of Physics, Graduate School of Science, The University of Tokyo, Tokyo 113-0033, Japan. [7]Department of Physics and Astronomy, Seoul National University, Seoul 151-742, Korea. [8]Department of Physics and Astronomy, University of California, Los Angeles, CA 90095, USA. [9]Korea Astronomy and Space Science Institute (KASI), Daejeon 305-348, Korea. [10]Institute of Astronomy and Astrophysics, Academia Sinica, Taipei 10617, Taiwan, Republic of China. [11]Frontier Research Institute for Interdisciplinary Science, Tohoku University, Sendai, Miyagi, 980-8578, Japan.
***Corresponding author. E-mail: jjb@astro.caltech.edu**

on a laboratory measurement, and masked for stars and galaxies using the Two Micron All Sky Survey (2MASS) *J*- and *H*-band catalogs (*15*). We analyze differences between fields to reduce the effect of flat-fielding errors. The auto- and cross-power spectra of the masked, differenced images, corrected for mode coupling from the mask using a correction matrix, are shown in Fig. 1. We also compute auto- and cross-spectra from a Spitzer infrared array camera (IRAC) 3.6-μm image that coincides with two of the five CIBER fields.

The CIBER auto- and cross-spectra show a significant excess over the predicted fluctuations from known galaxy populations (*16*) at $l < 5000$, where the multipole moment $l \cong \pi/\theta$, and θ is the angular separation of two points on the sky. The excess is also evident in the cross-power spectra with Spitzer, showing that the source of the fluctuations is largely common from 1.1 to 3.6 μm. The large-scale fluctuations measured with CIBER correlate between the two flights in all combinations of bands and are independent of the detector arrays; the data pass multiple internal consistency tests (see the supplementary materials).

We rule out the following sources for producing the large-scale fluctuations (Fig. 1): (i) sunlight scattered by interplanetary dust, (ii) starlight scattered by interstellar dust (known as diffuse Galactic light), and (ii) fluctuations from faint stars. Zodiacal light fluctuations are eliminated because we observed the same fields separated by 17 months and obtained consistent results, viewed through two independent lines of sight through the interplanetary dust cloud. Constraints on zodiacal light fluctuations from Spitzer at 8 μm (*8*), scaled by the zodiacal spectrum to near-infrared wavelengths (*17*), lie significantly below the detected fluctuations (Fig. 1). The zodiacal spectrum is scaled by a conservative upper limit to the fluctuation amplitude measured at 7 μm from AKARI (*17*, *18*) in Fig. 2.

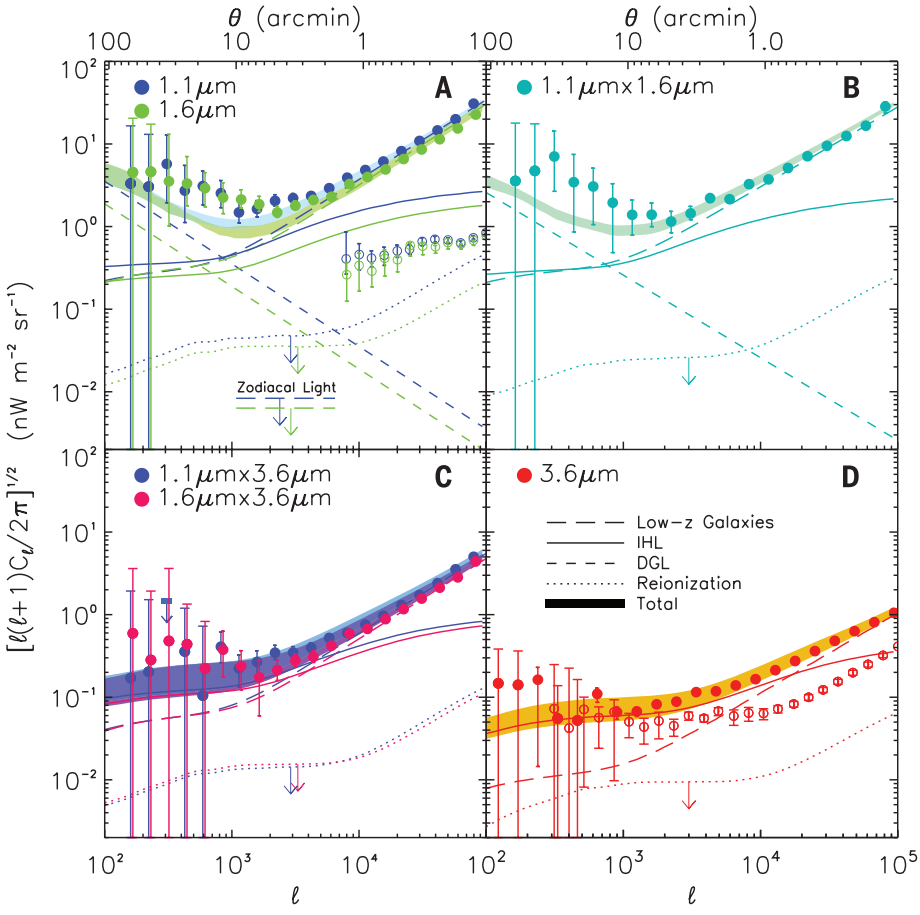


**Fig. 1. CIBER and Spitzer auto- and cross-spectra at 1.1, 1.6 and 3.6 μm.** We show the CIBER auto-spectra for 1.1 by 1.1 μm, and 1.6 by 1.6 μm (**A**), the CIBER 1.1 by 1.6 μm cross-spectrum (**B**), the CIBER-Spitzer 1.1 by 3.6 μm and 1.6 by 3.6 μm cross-spectra (**C**), and the Spitzer 3.6 by 3.6 μm auto-spectra (*6*) (**D**). At 1.1, 1.6, and 3.6 μm, we indicate previous measurements [open circles; (*6*, *10*); note that the Hubble measurements apply a much deeper flux cut at 1.1 and 1.6 μm for masking and that the Spitzer flux cut is somewhat deeper than the cut we are applying at 3.6 μm]. The 3.6-μm points use the same data set but are masked to a lower source flux for comparison to our spectrum, which is masked to $L < 16$. The increased depth reduces some of the mid-$l$ power. We show constraints on astrophysical foregrounds, including unmasked stars and $z < 5$ galaxies (*16*), zodiacal light (*8*), and diffuse Galactic light. In all cases, we detect a significant excess power at $l < 5000$ (angular separations $\theta > 4.3'$). We model the data using components from IHL (*6*) and $z > 7$ first galaxies (*3*, *5*), obtaining a 95% confidence upper limit on the EOR contribution. The fitted total indicated by the filled band includes all of the astrophysical components plus a bounded systematic error for flat-field variations. The width of the band indicates the 68% uncertainty interval of the fit, including all of the modeling uncertainties. The correlation coefficients for 1.1 by 1.6 μm, 1.1 by 3.6 μm, and 1.6 by 3.6 μm are 0.76 ± 0.10, 0.55 ± 0.14 and 0.31 ± 0.14, respectively, with no statistically significant angular dependence in the correlations (see section 6.2 of the supplementary materials for a description of this calculation).

We estimate diffuse Galactic light fluctuations (Figs. 1 and 2) by scaling the Infrared Astronomical Satellite (IRAS) 100-μm intensity by a factor consistent with previous diffuse Galactic light measurements (*19*). We estimate the diffuse Galactic light component by calculating the CIBER–IRAS cross-spectra and fitting a single amplitude coefficient to a $C_l \propto l^{-3}$ spectrum with a fixed 1.1 μm / 1.6 μm color ratio, which is less than the detected CIBER power spectra at all spatial scales. Fluctuations from the extinction of the background light by galactic dust are also negligible.

We constrain fluctuations from unmasked stars using the UKIDSS-UDS stellar catalog (*20*), which is complete to $J = 24.9$, $H = 24.2$ (5 σ), accounting for > 99.9% of the integrated light from stars. We compute the autopower spectrum of residual stars below our cutoff flux and find that the amplitude is negligible on large scales and follows a Poisson spectrum.

The root mean square (RMS) fluctuation amplitude $\delta\lambda I_\lambda = \langle l(l+1)C_l/2\pi\rangle^{1/2}$ over $500 < l < 2000$ has a spectral energy distribution that is approximately Rayleigh-Jeans (Fig. 2). The 1.1-μm data point lies 2σ below the best-fitting $\lambda^{-3}$ scaling, suggesting the possibility of a departure from the Rayleigh-Jeans spectrum at short wavelengths. To fit models to CIBER and Spitzer data, we mask Spitzer data to a depth $L < 16$ that is comparable to CIBER. The Spitzer power spectra give a non-Poissonian $l^{1.7}$ signal at high multipoles for the $L < 16$ flux cut (Fig. 1), which is evidence for nonlinear clustering that is not observed with a deeper flux cut (*6*) and is not predicted in linear galaxy clustering (*16*).

Having excluded explanations based on zodiacal light, diffuse Galactic light, and the clustering of known galaxies, we consider three possibilities to explain these measurements: EOR galaxies, EOR black holes, and IHL. For first-light galaxies, we use models for population II and population III stars (*21*) and combinations of the two. The direct-collapse black hole model at $z > 12$ is excluded both by amplitude and color, as it has no mechanism to generate substantial 1.1- and 1.6-μm power (*4*). For IHL, we use models based on the spectral energy distributions of old stellar populations in dark matter halos (*6*). We simultaneously fit the 1.1-, 1.6-, and 3.6-μm autopower spectra, taking into account galaxy clustering, diffuse Galactic light, and residual flat-field errors at low $l$. The IHL model, summarized in Fig. 1, generally fits the data but somewhat underpredicts the amplitude at 1.1 and 1.6 μm; neither the

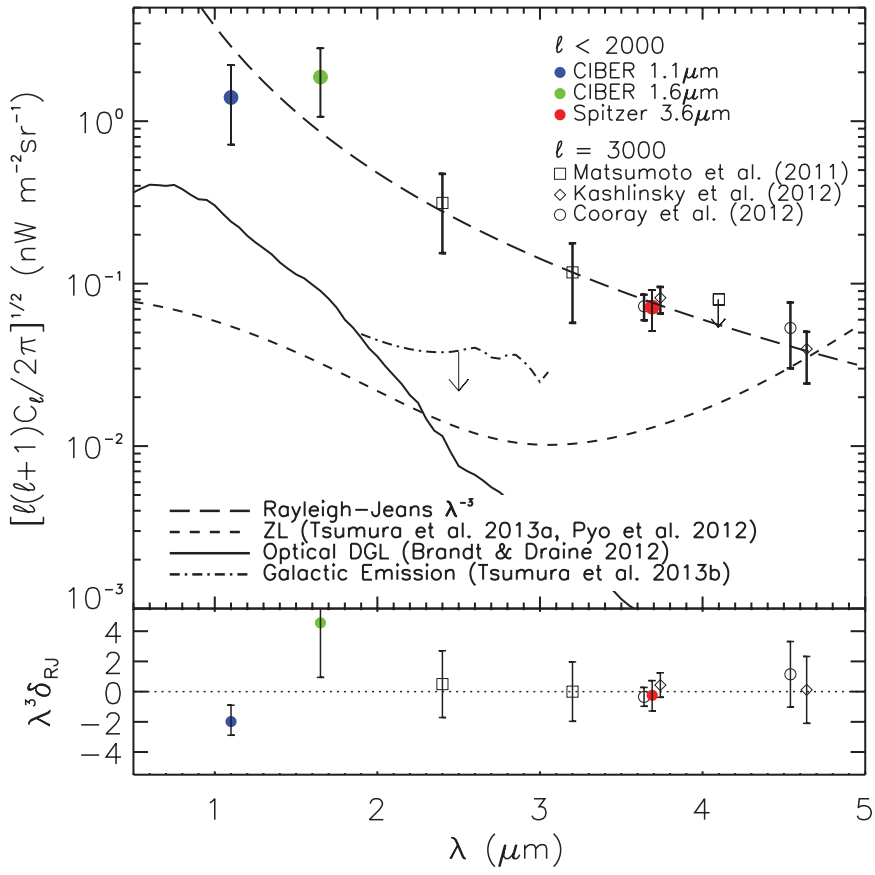


**Fig. 2. The electromagnetic spectrum of the near-infrared fluctuations.** We show measurements of the fluctuation power from CIBER and Spitzer averaged between 500 < $\ell$ < 2000 (solid points). Also indicated are previous measurements from AKARI (*11*) and Spitzer (*6*, *7*) at $\ell$ = 3000 that use deeper masking thresholds. In all cases, we subtract the contribution from the shot noise of unmasked galaxies (*16*). We indicate the best-fitting Rayleigh-Jeans spectrum to the points from this analysis, estimates for diffuse Galactic light fluctuations (*19*), a conservative constraint on zodiacal light fluctuations (*17*, *18*), and an upper limit on Galactic emission (*27*). The known foreground components have both smaller amplitudes and different spectra than the measurements. We show the residual from the best-fitting Rayleigh-Jeans spectrum $\delta_{RJ}$ in the bottom panel, scaled by $\lambda^3$ to reduce the range. The shortest wavelength measurement at 1.1 μm is 2.0 σ below the fit, indicating a possible short-wavelength departure from a Rayleigh-Jeans spectrum.

**Table 1. Contributions to near-infrared EBL anisotropy and intensity.** At each wavelength, we list the measured fluctuation amplitude at large angular scales; the model-dependent ratio of EBL intensity to EBL anisotropy; the IGL determined by previous measurements; the ratio of the IHL and IGL intensities; and finally, the inferred total background intensity from both components. We also list the background intensity that would arise assuming the measured fluctuations are entirely due to high-redshift EOR galaxies.

| λ (μm) | Measured $\delta\lambda I_\lambda$* (nW m$^{-2}$ sr$^{-1}$) | $\frac{\lambda I_{\lambda,\mathrm{IHL}}}{\delta\lambda I_\lambda}$ | $\lambda I_{\lambda,\mathrm{IHL}}$‡ (nW m$^{-2}$ sr$^{-1}$) | $\lambda I_{\lambda,\mathrm{IGL}}$§ (nW m$^{-2}$ sr$^{-1}$) | $\frac{\lambda I_{\lambda,\mathrm{IHL}}}{\lambda I_{\lambda,\mathrm{IGL}}}$ | $\lambda I_{\lambda,\mathrm{IHL}} + \lambda I_{\lambda,\mathrm{IGL}}$ (nW m$^{-2}$ sr$^{-1}$) | $\lambda I_{\lambda,\mathrm{EOR}}$‖ (nW m$^{-2}$ sr$^{-1}$) |
|---|---|---|---|---|---|---|---|
| 1.1 | $1.4^{+0.8}_{-0.7}$ | 5 | $7.0^{+4.0}_{-3.5}$ | $9.7^{+3.0}_{-1.9}$ | 0.7 | $16.7^{+5.0}_{-4.0}$ | 28 |
| 1.6 | $1.9^{+0.9}_{-0.8}$ | 6 | $11.4^{+5.4}_{-4.8}$ | $9.0^{+2.6}_{-1.7}$ | 1.3 | $20.4^{+6.0}_{-5.1}$ | 38 |
| 2.4 | 0.32 ± 0.05† | 7 | 2.2 ± 0.4 | $7.8^{+2.0}_{-1.2}$¶ | 0.3 | $10.0^{+2.0}_{-1.3}$ | 6.4 |
| 3.6 | $0.072^{+0.019}_{-0.021}$ | 9 | $0.65^{+0.17}_{-0.19}$ | 5.2 ± 1.0 | 0.1 | 5.9 ± 1.0 | 1.4 |
| 3.6# | $0.049^{+0.021}_{-0.007}$ | 9 | $0.44^{+0.19}_{-0.06}$ | 5.2 ± 1.0 | 0.1 | 5.6 ± 1.0 | 1.0 |
| 4.5 | 0.053 ± 0.023† | 7 | 0.37 ± 0.16 | 3.9 ± 0.8 | 0.1 | 4.3 ± 0.8 | 1.0 |

*RMS fluctuation amplitude computed as averages of measured data over 500 < $\ell$ < 2000, except for those marked †, which are determined at $\ell$ = 3000 using fainter mask cuts due to restricted field size (see also note ||). ‡The IHL background from the product of columns 2 and 3. §The IGL background as compiled by (*28*). ||Computed EOR background assuming EOR fluctuations with $\lambda I_\lambda/\delta\lambda I_\lambda$ = 20. ¶Determined at *K* band corresponding to 2.2 μm. #Computed using the measurements of (*6*) averaged over 500 < $\ell$ < 5000.

IHL nor the EOR models quite match the high observed 1.6-/3.6-μm color ratio (see section 10 of the supplementary materials). This may indicate that additional components are reflected in the data. However, more theoretical work is required to determine whether adding nonlinear galaxy clustering and nonlinear IHL production to the model can improve the fit.

We estimate the EBL intensity associated with the fluctuations by taking the measured fluctuation amplitude between 500 < $\ell$ < 2000, obtained by subtracting estimated contributions from low-$z$ galaxies and diffuse Galactic light, and multiplying by a model-dependent contrast factor $\lambda I_\lambda/\delta\lambda I_\lambda$, where $\lambda I_\lambda$ is the total intensity associated with a component. For the IHL model, which has a low contrast factor, we obtain an associated EBL of $7.0^{+4.0}_{-3.5}$ and $11.4^{+5.4}_{-4.8}$ nW m$^{-2}$ sr$^{-1}$ at 1.1 and 1.6 μm, respectively. As shown in Table 1, the IHL background is of a similar magnitude to the integrated galaxy light (IGL) background derived from galaxy counts. However, we note that the IHL background has a much bluer color than the IGL background. We similarly estimate the IHL background at longer wavelengths from AKARI and Spitzer. Nonlinear galaxy clustering appears to contribute to the Spitzer fluctuations, so we quote two values that depend on the choice of flux cut, the deeper flux cut being less sensitive to the nonlinear clustering contribution. The CIBER data do not appear to be as sensitive to the flux cut, perhaps due to the higher IHL to IGL ratio at these wavelengths.

The total EBL, the summation of the IHL and IGL backgrounds, is consistent with current EBL measurements. Near-infrared absolute photometric background measurements remain uncertain due to the bright zodiacal foreground, but the lowest such measurement (*22*) gives 21 ±15 nW m$^{-2}$ sr$^{-1}$ and 13.3 ± 2.8 nW m$^{-2}$ sr$^{-1}$ at 1.25 and 3.6 μm, respectively. The High Energy Stereoscopic System (HESS) measurement of the EBL using γ-ray

absorption spectra (*23*), 15 ± 2 (statistical) ± 3 (systematic) nW $m^{-2}$ $sr^{-1}$ at 1.4 μm, is independently consistent with the sum of the IHL and IGL backgrounds, within the uncertainties in all measurements.

An EOR interpretation of these measurements would result in a large background, as the contrast factor is larger than that of IHL, 10 to 100 for EOR models (*3*, *6*). The implied EOR background (see Table 1) originating from high redshifts is difficult to justify due to the overproduction of metals and x-ray background photons (*24*).

Our results indicate that a substantial fraction of the EBL at optical and near-infrared wavelengths originates from stars outside of galaxies (with boundaries as traditionally defined). This in turn adds to the cosmic energy budget and, depending on the mass characteristics and spectrum of the population responsible, could help alleviate the "photon underproduction crisis" (*25*) and the "missing baryon problem" (*26*). We see no evidence for a detected EOR background component in our data. Multiwavelength fluctuation measurements extending into the optical will help discriminate the EOR background component using the redshifted Lyman cutoff, and future spectroscopic measurements will enable tomographic measurements to determine the history of IHL production.

## REFERENCES AND NOTES


1. A. Cooray, J. J. Bock, B. Keatin, A. E. Lange, T. Matsumoto, *Astrophys. J.* **606**, 611–624 (2004).
2. A. Kashlinsky, R. Arendt, J. P. Gardner, J. C. Mather, S. H. Moseley, *Astrophys. J.* **608**, 1–9 (2004).
3. E. R. Fernandez, E. Komatsu, I. T. Iliev, P. R. Shapiro, *Astrophys. J.* **710**, 1089–1110 (2010).
4. B. Yue, A. Ferrara, R. Salvaterra, Y. Xu, X. Chen, *Mon. Not. R. Astron. Soc.* **433**, 1556–1566 (2013).
5. A. Cooray, Y. Gong, J. Smidt, M. G. Santos, *Astrophys. J.* **756**, 92 (2012).
6. A. Cooray *et al.*, *Nature* **490**, 514–516 (2012).
7. A. Kashlinsky, R. G. Arendt, J. Mather, S. H. Moseley, *Nature* **438**, 45–50 (2005).
8. A. Kashlinsky, R. G. Arendt, J. Mather, S. H. Moseley, *Astrophys. J.* **654**, L5–L8 (2007).
9. A. Kashlinsky *et al.*, *Astrophys. J.* **753**, 63 (2012).
10. R. I. Thompson, D. Eisenstein, X. Fan, M. Rieke, R. C. Kennicutt, *Astrophys. J.* **666**, 658–662 (2007).
11. T. Matsumoto *et al.*, *Astrophys. J.* **742**, 124 (2011).
12. N. Cappelluti *et al.*, *Astrophys. J.* **769**, 68 (2013).
13. M. Zemcov *et al.*, *Astrophys. J. Suppl. Ser.* **207**, 31 (2013).
14. J. Bock *et al.*, *Astrophys. J. Suppl. Ser.* **207**, 32 (2013).
15. M. F. Skrutskie *et al.*, *Astron. J.* **131**, 1163–1183 (2006).
16. K. Helgason, M. Ricotti, A. Kashlinsky, *Astrophys. J.* **752**, 113 (2012).
17. K. Tsumura *et al.*, *Publ. Astron. Soc. Japan* **65**, 119 (2013).
18. J. Pyo, T. Matsumoto, W.-S. Jeong, S. Matsuura, *Astrophys. J.* **760**, 102 (2012).
19. T. D. Brandt, B. T. Draine, *Astrophys. J.* **744**, 129 (2012).
20. A. Lawrence *et al.*, *Mon. Not. R. Astron. Soc.* **379**, 1599–1617 (2007).
21. E. R. Fernandez, E. Komatsu, *Astrophys. J.* **646**, 703–718 (2006).
22. L. R. Levenson, E. L. Wright, B. D. Johnson, *Astrophys. J.* **666**, 34–44 (2007).
23. H.E.S.S. Collaboration., *Astron. Astrophys.* **550**, A4 (2013).
24. P. Madau, J. Silk, *Mon. Not. R. Astron. Soc.* **359**, L37–L41 (2005).
25. J. A. Kollmeier *et al.*, *Astrophys. J.* **789**, L32 (2014).
26. M. Fukugita, C. J. Hogan, P. J. E. Peebles, *Astrophys. J.* **503**, 518–530 (1998).
27. K. Tsumura *et al.*, *Proc. Astron. Soc. Japan* **65**, 120 (2003).
28. A. Franceschini, G. Rodighiero, M. Vaccari, *Astron. Astrophys.* **487**, 837–852 (2008).



## ACKNOWLEDGMENTS

Our thanks to O. Doré, J. Filippini, and K. Ganga for useful conversations and comments throughout the course of this work and K. Helgason for kindly providing models of the statistics of the near-infrared CIB. The authors acknowledge the excellent support from the NASA sounding rockets program that was essential in developing, testing, qualifying, launching, and recovering our payloads. The CIBER auto- and cross-power spectra are available for public download at http://ciber.caltech.edu/zemcovetal. This work was supported by NASA APRA research grants NNX07AI54G, NNG05WC18G, NNX07AG43G, NNX07AJ24G, and NNX10AE12G. Initial support was provided by an award to J.B. from the Jet Propulsion Laboratory's Director's Research and Development Fund. Japanese participation in CIBER was supported by KAKENHI (20·34, 18204018, 19540250, 21340047, and 21111004) from Japan Society for the Promotion of Science (JSPS) and the Ministry of Education, Culture, Sports, Science and Technology (MEXT). Korean participation in CIBER was supported by the Pioneer Project from Korea Astronomy and Space Science Institute (KASI). M.Z. and P.K. acknowledge support from NASA Postdoctoral Program fellowships, A.C. acknowledges support from an NSF CAREER award AST-0645427 and NSF AST-1313319, and K.T. acknowledges support from the JSPS Research Fellowship for Young Scientists. This publication makes use of data products from the Two Micron All Sky Survey (2MASS), which is a joint project of the University of Massachusetts and the Infrared Processing and Analysis Center/California Institute of Technology, funded by the National Aeronautics and Space Administration and the National Science Foundation. This work made use of images and/or data products provided by the National Optical Astronomy Observatory (NOAO) Deep Wide-Field Survey (NDWFS), which is supported by NOAO, operated by AURA, Inc., under a cooperative agreement with the National Science Foundation.


## SUPPLEMENTARY MATERIALS

www.sciencemag.org/content/346/6210/732/suppl/DC1
Materials and Methods
Supplementary Text
Figs. S1 to S27
Tables S1 to S2
References (*29*–*55*)

1 July 2014; accepted 3 October 2014
10.1126/science.1258168

EARLY EARTH

# Sulfate was a trace constituent of Archean seawater

**Sean A. Crowe,[1,2]*† Guillaume Paris,[3]* Sergei Katsev,[4] CarriAyne Jones,[1,2] Sang-Tae Kim,[5] Aubrey L. Zerkle,[6] Sulung Nomosatryo,[7] David A. Fowle,[8] Jess F. Adkins,[3] Alex L. Sessions,[3] James Farquhar,[9] Donald E. Canfield[2]**

**In the low-oxygen Archean world (>2400 million years ago), seawater sulfate concentrations were much lower than today, yet open questions frustrate the translation of modern measurements of sulfur isotope fractionations into estimates of Archean seawater sulfate concentrations. In the water column of Lake Matano, Indonesia, a low-sulfate analog for the Archean ocean, we find large (>20 per mil) sulfur isotope fractionations between sulfate and sulfide, but the underlying sediment sulfides preserve a muted range of $\delta^{34}S$ values. Using models informed by sulfur cycling in Lake Matano, we infer Archean seawater sulfate concentrations of less than 2.5 micromolar. At these low concentrations, marine sulfate residence times were likely $10^3$ to $10^4$ years, and sulfate scarcity would have shaped early global biogeochemical cycles, possibly restricting biological productivity in Archean oceans.**

Sulfur interacts with carbon and oxygen in global biogeochemical cycles that regulate Earth's surface chemistry and biology (*1*). At 28 mM, sulfate is abundant in modern seawater, fueling extensive sedimentary microbial sulfate reduction (MSR) (*2*). At these concentrations, MSR typically imparts large sulfur isotope fractionations (*3*), allowing the use of sulfur isotopes to reconstruct past global change (*4*, *5*). Small sulfur isotope fractionations preserved in bulk pyrite from Archean (>2400 million years ago) rocks led to the original conclusion that the Archean oceans contained <200 μM sulfate, or ~1% of modern seawater (*5*). The distribution of mass-independent sulfur isotopes in Archean sediments (*4*, *6*–*8*) and box models of global sulfur cycling (*9*) imply even lower Archean seawater sulfate of <60 to 80 μM. Paradoxically, microscale sulfur isotope data from Archean pyrites (*10*–*12*) reveal large sulfur isotope fractionations of up to 40 per mil (‰) in the Archean—fractionations only seen at hundreds to thousands of micromolar sulfate in modern environments (*13*–*15*). Electron-donor availability (*3*, *16*) and MSR rate (*3*, *16*, *17*), however, also exert influence, with larger fractionation typically imparted when electron donors limit sulfate-reduction rates, allowing the

[1]Department of Microbiology and Immunology and Department of Earth, Ocean, and Atmospheric Sciences, University of British Columbia, Vancouver, British Columbia, Canada. [2]NordCEE and Department of Biology, University of Southern Denmark, Odense, Denmark. [3]Department of Geological and Planetary Sciences, California Institute of Technology, Pasadena, CA 91125, USA. [4]Large Lakes Observatory and Department of Physics, University of Minnesota, Minneapolis, MN 55812, USA. [5]School of Geography and Earth Sciences, McMaster University, Hamilton, Ontario, Canada. [6]Department of Earth and Environmental Sciences, University of St. Andrews, St. Andrews, UK. [7]Research Center for Limnology, Indonesian Institute of Sciences, Cibinong, West Java, Indonesia. [8]Department of Geology, University of Kansas, Lawrence, KS 66045, USA. [9]Department of Geology, University of Maryland, College Park, MD 20742, USA.
*These authors contributed equally to this work. **†Corresponding author. E-mail: sacrowe1@gmail.com**